Contour Instabilities in Early Tumor Growth Models

M. Ben Amar, C. Chatelain, and P. Ciarletta

Laboratoire de Physique Statistique, Ecole Normale Supérieure, UPMC Univ Paris 06, Université Paris Diderot, CNRS, 24 rue Lhomond, 75005 Paris, France

(Received 16 November 2010; published 4 April 2011)

Recent tumor growth models are often based on the multiphase mixture framework. Using bifurcation theory techniques, we show that such models can give contour instabilities. Restricting to a simplified but realistic version of such models, with an elastic cell-to-cell interaction and a growth rate dependent on diffusing nutrients, we prove that the tumor cell concentration at the border acts as a control parameter inducing a bifurcation with loss of the circular symmetry. We show that the finite wavelength at threshold has the size of the proliferating peritumoral zone. We apply our predictions to melanoma growth since contour instabilities are crucial for early diagnosis. Given the generality of the equations, other relevant applications can be envisaged for solving problems of tissue growth and remodeling.

DOI: 10.1103/PhysRevLett.106.148101 PACS numbers: 87.19.xj, 47.20.Ky, 47.61.Jd, 87.18.Hf

Introduction.—Soft tissue growth models in ideal geometries have shown shape instabilities with a special focus on morphogenesis of living systems [1–3]. Anisotropic or inhomogeneous growth and constraints due to boundaries are responsible for these shape instabilities. Most models explore the mechanical properties with perhaps an excessive simplification of the growth process itself. On the contrary, after several decades since the pioneering work of Greenspan [4], tumor growth models have explored all the facets of possible elementary biological processes known to date [5] with different modeling approaches at different scales: continuum models at the tissue scale, discrete models at the cells scale, and eventually hybrid continuum-discrete models [6]. The recent review by [6] reports more than 550 citations but few of them explore the possibility of shape instabilities except in simplified models [4,7]. However, models based on nonlinear coupled partial-differential equations (PDEs) require numerical investigations [8,9] with lack of understanding of the parameters at the origin of shape instabilities.

Nevertheless, these instabilities are often correlated with the beginning of aggressive neoplasia: they are of utmost importance for melanoma where symmetry and regularity are key criteria in clinical methods [10]. Our aim is then to identify the main biophysical interactions at the origin of these contour instabilities. It has already been shown, both *in vitro* [11,12] and theoretically [13], that mechanical interactions between cells and their microenvironment are crucial for tumor evolution and can determine some macroscopic tumor properties [11].

We discuss here how they can control tumor shape evolution as well, dictating the condition for the development of contour instabilities on a circular growing tumor, possibly giving rise to the patterns observed *in vivo*. We consider a continuous multiphase model describing the tumor as a two component mixture [6]. Although simplificative, such a model already contains the main ingredients: a complex spectrum of cell-to-cell interactions, the elasticity of the tissue and the spatial availability of diffusing nutrients responsible for growth inhomogeneities inside the tumor.

We show explicitly that instabilities are governed mostly by the cell-cell interactions inside the tumor and we establish analytically an instability criterion for tumor growth. We compare our findings with clinical data on healthy skin and melanoma lesions. Although much more difficult to establish than standard instability criterions, e.g., appearing in classical pattern formation as the Rayleigh -Bénard [14] or the Mullins-Sekerka instability [15], our criterion has the potential to be a useful tool for predicting pattern formation in early epithelium tumor growth.

Formalism.—We model the radial two-dimensional growth of a soft tissue by a mixture of two phases, a proliferating cellular phase (volume fraction ϕ_c and velocity $\boldsymbol{v}_c$) and an interstitial liquid phase (ϕ_l, $\boldsymbol{v}_l$) in which nutrients, with concentration n, diffuse from the outer border of the tumor (healthy tissue). Considering the velocities involved in tumor growth [16,17], the nutrient advection is negligible, if compared to the diffusion, so that their transport is simply described by a diffusion consumption equation $\partial n/\partial t = D_n \Delta n - \delta_n \phi_c n$. Cellular growth depends linearly on the local nutrient concentration [18], a limiting factor being oxygen supply [19] causing often hypoxia and necrosis of the tumor center [20]. Cell death rate is taken constant, giving the volume transfer rate from liquid to cellular phase $\Gamma(\phi_c, n) = \gamma_c \phi_c n - \delta_c \phi_c$. The cellular phase is described as an elastic fluid with a stress tensor $\boldsymbol{T}_c$ defined by the constitutive equation $\boldsymbol{T}_c = [-\phi_c p - \Sigma(\phi_c)]\boldsymbol{I}$ where p is the hydrostatic pressure of the mixture and $-\Sigma(\phi_c)\boldsymbol{I}$ is the excess Cauchy stress, characterizing cell-to-cell interaction [17]. For physical and biological consistency, $\Sigma(\phi_c)$ has to vanish for $\phi_c \to 0$, to be negative for $\phi_c < \phi_e$ (attraction due to chemotaxis, haptotaxis, and cell adhesion), positive for $\phi_c > \phi_e$,

and to diverge for $\phi_c \to 1$ showing a strong repulsion at high cancerous cell concentration [see Fig. 2(a)]. The choice of such potential interaction [21], which reminds us of the Lennard-Jones potential valid for a vast class of atoms and molecules, may induce a spinodal decomposition inside the tumor and some mathematical problems, which are discussed in [22]. This difficulty is circumvented by choosing a compact initially spreading tumor $\phi_c > \phi_e$. Finally we consider a viscous interaction between the two phases $\boldsymbol{f}_{lc} = -\boldsymbol{f}_{cl} = M(\boldsymbol{v}_l - \boldsymbol{v}_c) + p\boldsymbol{\nabla}\phi_c$, described by a friction parameter M that gives a Darcy law $\boldsymbol{v}_c = -K(\phi_c)\boldsymbol{\nabla}\Sigma$ in a regime of negligible inertia, with the porosity coefficient $K(\phi_c) = M^{-1}(1-\phi_c)^2$. The boundary conditions at the tumor border $\boldsymbol{x}_b$ are $n(\boldsymbol{x}_b) = n_e$ and $\phi(\boldsymbol{x}_b) = \phi_e$ with $\Sigma(\phi_e) = 0$, ensuring a stress-free boundary. Evolution of the border is given by continuity of the velocity [23]. The governing equations can be rewritten in terms of the dimensionless quantities $\bar{x} = \sqrt{\delta_n/D_n}x$, $\bar{t} = \delta_n t$, $\bar{n} = n/n_e$ with $\bar{\Sigma} = \chi^{-1}\Sigma$ and χ a typical stress for cell-to-cell interaction. Dropping the bars for the dimensionless quantities and the subscripts concerning the cell phase in the following, the governing equations are

$$\frac{\partial\phi}{\partial t} + \boldsymbol{\nabla}\cdot(\phi\boldsymbol{v}) = \gamma\phi n - \delta\phi, \quad \text{with } \phi(\boldsymbol{x}_b) = \phi_e, \quad (1)$$

$$\frac{\partial n}{\partial t} = \Delta n - \phi n, \quad \text{with } n(\boldsymbol{x}_b) = 1, \quad (2)$$

$$\boldsymbol{v} = -D(1-\phi)^2\boldsymbol{\nabla}\Sigma, \quad \text{with } v(\boldsymbol{x}_b) = V_e, \quad (3)$$

with the dimensionless parameters $D = \chi/(MD_n)$, $\gamma = \gamma_c n_e/\delta_n$ and $\delta = \delta_c/\delta_n$. Experimental values and comparisons with clinical observations are discussed thereafter in the case of melanoma where atmospheric oxygen is the main source of nutrients [19].

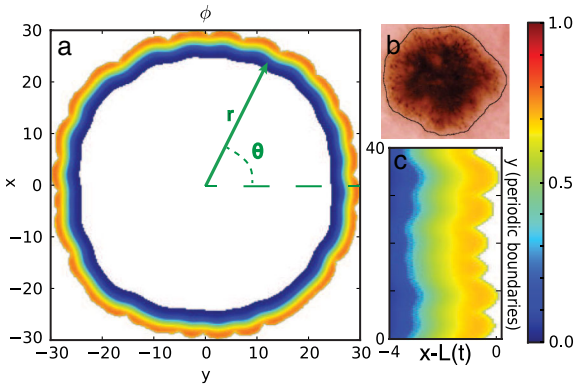

FIG. 1 (color online). (b) Malignant melanoma with irregular contour: courtesy of Dr H. Kittler (Dept for Dermatology, University of Vienna) and Dr P. Guitera (Sydney Melanoma Diagnostic Center). (a),(c) Tumor cell fraction ϕ and front instability in radial (a) and linear (c) geometry. Dimensionless parameters are: $\gamma = 0.05$, $\delta = 0.02$, $D = 0.2$, $\phi_e = 0.6$ with $\Sigma(\phi) = \phi^3(\phi - \phi_e)/(1-\phi)$.

Stability analysis.—First, and for simplicity, we begin with a one-dimensional tumor represented by a planar front at $x = L(t)$ propagating along the x axis [Fig. 1(c)]. The radial tumor growth is transformed into a planar one by means of a conformal mapping of the physical plane. The numerical simulations reveal [Fig. 2(b)] the existence of steady travelling wave solutions with constant velocity U, developing a necrotic core ($\phi_0 \to 0$) in agreement with clinical observations [16]; but for a range of physical parameters, these solutions exhibit an instability along the y axis, that grows and saturates at a certain size [Fig. 1(c)]. In other words, it seems that a static wavy undulation is transported by the tumor front during its propagation along the x axis. To understand this particular front destabilization we perform a classical stability analysis of both fields ϕ and n with an infinitesimal perturbation ($\epsilon \ll 1$) of wave number κ such that $L = L_0 + \epsilon e^{\lambda t}\cos(\kappa y)$, $\phi = \phi_0 + \epsilon e^{\lambda t} f(z)\cos(\kappa y)$ and $n = n_0 + \epsilon e^{\lambda t} g(z)\cos(\kappa y)$, with $z = x - Ut$. The sign of the eigenvalue λ, assumed real for viscous-elastic dynamics, gives the stability of the front to transverse perturbations. The long-wavelength limit ($\kappa \ll 1$) and the resulting phase

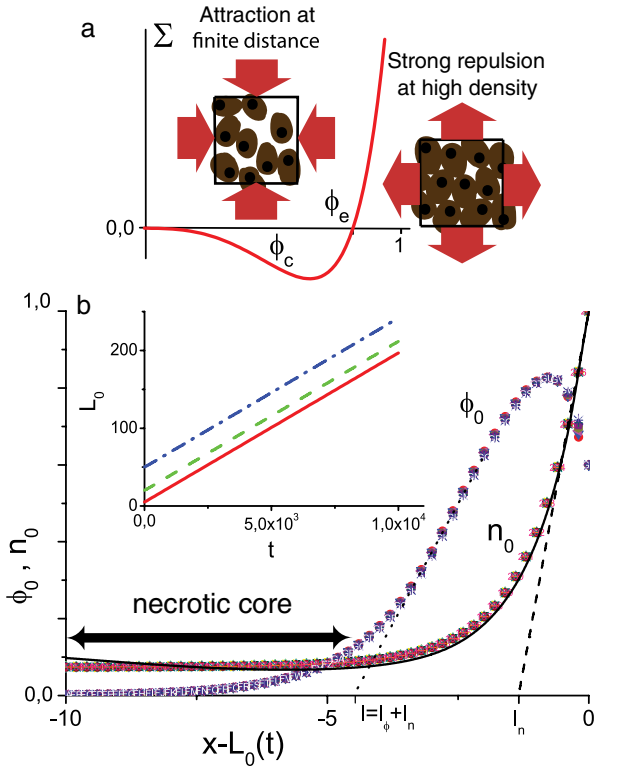

FIG. 2 (color online). (a) Biologically consistent cell-to-cell interaction, attractive below a volume fraction ϕ_e and repulsive above. (b) Cell volume fraction ϕ_0 and nutrient concentration n_0 in the moving referential $z = (x - L)$ associated to the tumor border $L(t)$ (dots) and WKB approximation [24] of n_0. In the inset linear growth of L independent of the initial size, $L(0) = 5$, 20, 50.

diagram have already been reported in [17]. However, the numerical instabilities usually appear before entering the unstable long-wavelength domain suggesting for the eigenvalue λ the scenario sketched in Fig. 3(a) typical of a symmetry breakdown with generation of a static periodic pattern. The definition of a typical finite wavelength $\Lambda = 2\pi/\kappa$ from our simulations is also coherent with this scenario (see Fig. 1). Using the change of function $\hat{f} = Gf \exp\left(-\int_z^0 U/(2G)dz'\right)$ with $G = D\phi_0 K(\phi_0) d\Sigma/d\phi_0$, we get for $\hat{f}$ at the leading order [17,24]

$$\hat{f}'' - [\kappa^2 + \zeta_\lambda(z)]\hat{f} = 0 \tag{4}$$

where $\zeta_\lambda(z) = UG'/(2G^2) + U^2/(4G^2) - (\gamma n_0 - \delta - \lambda)/G$. In the short wavelength limit (large κ) the nondiverging WKB solution of Eq. (4) satisfying the boundary condition Eq. (1) is $\hat{f} = -G(0)\phi_0'(0)\exp(\kappa z)$. The boundary condition Eq. (3) gives then $\lambda = G\phi_0'\kappa/\phi_0 < 0$ meaning that the short wavelength domain is always stable for any value of the parameters. The contour instabilities observed numerically appear for a finite κ given by $\lambda = d\lambda/d\kappa = 0$ as depicted by Fig. 3(a). For $\lambda = 0$ and after linearization, the boundary conditions given in the right of Eqs. (1) and (3) give the relation at $z = 0$

$$\frac{\hat{f}'}{\hat{f}} = \frac{-\phi_0'}{2\phi_0}(T-1) \quad \text{with } T = \frac{-2(\gamma-\delta)\phi_0}{\phi_0' U}. \tag{5}$$

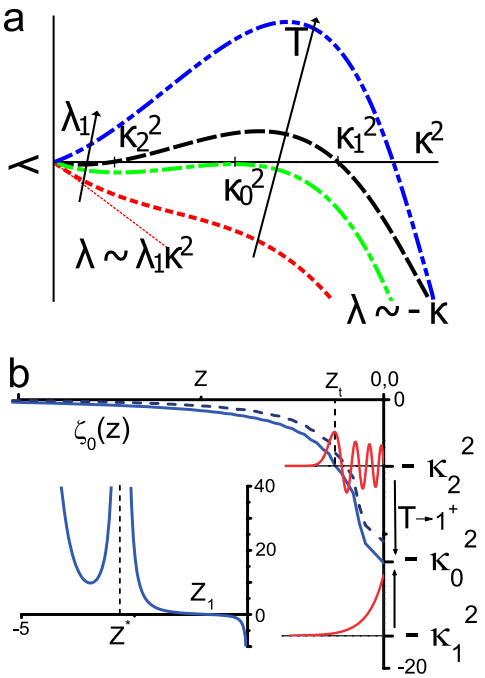

FIG. 3 (color online). (a) Phase diagram for the growth rate of instability. (b) Potential $\zeta_0(z)$ and its approximation by $(\phi_0'/\phi_0)^2$ (dashed line) at the tumor border. Two WKB solutions of Eq. (4) [24] for $\kappa_1^2 > -\zeta_0(0)$ and for $\kappa_2^2 < -\zeta_0(0)$. Values for parameters are $\gamma = 0.05$, $\delta = 0.02$, $D = 0.2$, $\phi_e = 0.6$.

Indeed Eq. (4) is analog to a Schrödinger equation for a quantum particle with a finite energy $-\kappa^2$ in the potential $\zeta_0(z)$. Figure 3(b) depicts this potential, which has a centrifugal barrier at $z = z*$ and a negative part near the tumor border. From quantum mechanics we know that the spectrum of eigenvalues is discrete and finite [25]. At the instability threshold this spectrum should reduce to a unique critical wavelength κ_0 as shown in Fig. 3(b). For $\kappa^2 > \kappa_0^2 = -\zeta_0(0)$, the nondiverging WKB solutions of Eq. (4) are $\hat{f}(z) = \hat{f}(0)\exp(-\int_z^0 \sqrt{\kappa^2 + \zeta_0(z')}dz')$ and Eq. (5) imposes $\sqrt{\kappa^2 + \zeta_0(0)} = -(\phi_0'/2\phi_0)(T-1)$. For $T > 1$ this solution gives a first root κ_1, as depicted in Fig. 3(b). For $\kappa < \kappa_0$ there exists a turning point where the WKB phase $S_\kappa' = \sqrt{-\kappa^2 - \zeta(z)}$ cancels and whose position z_t depends on the κ value [see Fig. 3(b)]. The required boundness of the solution, when the potential diverges like the centrifugal barrier for quantum states added to the presence of a turning point, imposes the WKB phase at $z = z_t$ which is very close to $\pi/4$ (convergent Airy function), and thus only a finite discrete set of κ values corresponds to wavy solutions satisfying Eq. (5): $S_\kappa' \mathrm{cotan}(\pi/4 + \int_{z_t}^0 S_\kappa' dz) = -(\phi_0'/2\phi_0)(T-1)$. For $0 < T - 1 \ll 1$ there is at least one κ value satisfying this relation that gives the second root κ_2 depicted in Fig. 3(b). For $T \to 1^+$ these two roots converge to κ_0 and disappear for $T < 1$. We conclude that T is the control parameter of the instability at finite wavelength and $2\pi/\kappa_0$ is the critical wavelength at instability threshold.

Since ζ_0 is scaled by $(\phi'/\phi)^2$ [24], the selected κ will be of an order $1/l_n$, l_n being the length scale of variation of the tumor concentration at the border so $\kappa \sim \sqrt{\phi_e}$. The penetration length of the instabilities inside the tumor is fixed by the position of the turning point z_t, close to the tumor border, which means that instabilities start in the external part of the tumor. The turning point $|z_1|$ for $\kappa = 0$ gives an upper bound for this penetration length which corresponds roughly to the position of the maximum of ϕ_0. Therefore nutrients and instability have the same typical penetration length l_n in the tumor. In physical units the main characteristics of the instability: the threshold T, the wavelength Λ and the instability penetration length l_n are then given by:

$$T = \frac{2\Gamma(\phi_e, n_e)K(\phi_e)}{V_e^2}\frac{d\Sigma}{d\phi_e}, \quad \Lambda \sim 2\pi l_n \sim \sqrt{\frac{4\pi^2 D_n}{\phi_e \delta_n}} \tag{6}$$

with $\Gamma(\phi_e, n_e) = (\gamma_c n_e - \delta_c)\phi_e$. For $\phi_e = 0$, i.e., no attraction between cells, $T = 0$ and the tumor front is always stable as found in the long-wavelength limit and various tumor models [17,26].

In the more realistic radial case, a necrotic core develops quickly, all the proliferative activity being confined in a ring of quasiconstant width l with a radius $R(t)$ growing linearly in time ($dR/dt = \dot{R} = U$) as observed *in vivo* [16] [Fig. 1(a)]. After the conformal transformation $z = R\log(r/R)$ and looking for slowing adiabatic solutions

with $|\dot{R}| \ll 1$, the radial growth is mapped to a planar growth along z and $2\pi R$ periodic along y and we recover very similar governing equations except a factor $\exp(-2z/R)$ and $1 - z/R$ in front of the divergence and the convective term, respectively. Performing the same stability analysis as for the planar case we get a similar equation as Eq. (4) for finite wavelength perturbations. For $\lambda = 0$ the value of the potential $\zeta_{0,R}$ at the tumor border can be written

$$\zeta_{0,R}(0) = \frac{U}{2G}\left(\frac{1}{R} - \frac{1}{R_c}\right) \tag{7}$$

with a critical radius $1/R_c = 2(\gamma - \delta)/U - G'/G - U/2G$. Above the instability threshold the first root κ_1 giving a solution satisfies $\sqrt{\kappa_1^2 + \zeta_{0,R}(0)} = -(\phi_0'/2\phi_0) \times (T - 1) - 1/R$ and we conclude that the tumor front is unstable for $T > 1$ but only after the tumor size reaches a critical radius that becomes infinite as $T \to 1$. One may think that the wavelength will collapse as time goes on. It is not true for such $\lambda(\kappa)$ diagram as presented in Fig. 3(b). Nonlinearities, out of reach of the present analysis, will bring the contour instability to saturation, fixing the structure of the pattern close to the aspect at threshold.

Discussion.—We have reported the first analytical proof for the existence of instabilities in front dynamics governed by multiphase mixture models. With a WKB treatment we identify a control parameter T, depending on tumor cell volume fraction at the border fixed by the cell-to-cell interaction potential, on the rate of cell growth (proliferation and oxygen consumption rates), and on the front velocity. The growth dynamics, for T larger than 1, reaches, after a transient time, a circular regime up to a threshold radius value. Later, instabilities start at the outer edge of the growing melanoma, and the wavelength of the undulated tumor front has the same typical length as the nutrient distribution.

Taking into account experimental values ([19] and references therein) for the model parameters ($\Gamma \sim 0.2$–$0.67\ \text{day}^{-1}$, $\delta_n \sim 1190$–$3030\ \text{day}^{-1}$, $D_n \sim 8.64$–$86.4\ \text{mm}^2\,\text{day}^{-1}$) we estimate the stability properties of different growing melanoma. Taking oxygen as the limiting nutrient [19], our model predicts for rapidly growing melanoma (i.e., nodular melanoma, having $V_e \sim 1.5\ \text{mm month}^{-1}$) a control parameter $T < 1$, a stable symmetrical growth, while for slowly growing melanoma types ($V_e = 0.12$–$0.4\ \text{mm month}^{-1}$, [16]) the control parameter is in the range $T = 0.95$–16.2, predicting contour instabilities localized in an outer ring of size comparable to the nutrient penetration length, typically 0.07–0.35 mm. The predicted threshold radius is less than 0.68 mm, to compare with the 3 mm threshold given in the ABCDE criteria [10], for a typical growth rate of 0.33 mm per month, suggesting that contour instabilities of melanoma are observable in the early growth of the tumor. Finally the numerical simulation of our model predicts that a growth rate for melanoma should be 0.13 mm per month and should vary linearly with the cells' proliferation rate, in agreement with clinical observations and histopathology analysis [16].

Conclusion.—We have established an analytical method for studying the stability properties of a class of coupled PDEs governing front evolution. It will allow us to foster understanding in more detailed models, exploring the connection between geometrical aspects of the tumor and cell phenotypes. Ultimately, the comprehension of the shape instability and the pattern formation in multiphase models is of utmost importance for a wide range of problems relating to tissue growth, remodeling, and morphogenesis.

[1] A. Goriely and M. Ben Amar, Phys. Rev. Lett. **94**, 198103 (2005).
[2] J. Dervaux and M. Ben Amar, Phys. Rev. Lett. **101**, 068101 (2008).
[3] E. Efrati, E. Sharon, and R. Kupferman, Phys. Rev. E **80**, 016602 (2009).
[4] H. P. Greenspan, J. Theor. Biol. **56**, 229 (1976).
[5] C. Verdier *et al.*, C.R. Physique **10**, 790 (2009).
[6] J. S. Lowengrub *et al.*, Nonlinearity **23**, R1 (2010).
[7] H. M. Byrne and M. A. J. Chaplain, Eur. J. Appl. Math. **8**, 639 (1997).
[8] P. Macklin and J. S. Lowengrub, J. Theor. Biol. **245**, 677 (2007).
[9] V. Cristini *et al.*, J. Math. Biol. **58**, 723 (2008).
[10] H. Kittler *et al.*, Archives of Dermatology **142**, 1113 (2006).
[11] T. Roose *et al.*, Microvasc. Res. **66**, 204 (2003).
[12] G. Helmlinger *et al.*, Nat. Biotechnol. **15**, 778 (1997).
[13] M. A. J. Chaplain, L. Graziano, and L. Preziosi, Math. Med. Biol. **23**, 197 (2006).
[14] F. Charru, *Instabilités Hydrodynamiques (Hydrodynamic Instabilities)* (CNRS Editions, EDP Sciences, Paris, 2009).
[15] J. S. Langer, Rev. Mod. Phys. **52**, 1 (1980).
[16] W. Liu, Archives of Dermatology **142**, 1551 (2006).
[17] P. Ciarletta, L. Foret, and M. Ben Amar, J. R. Soc. Interface **8**, 345 (2010).
[18] K. A. O. Ellem and G. F. Kay, J. Cell Sci. **62**, 249 (1983).
[19] S. Eikenberry, C. Thalhauser, and Y. Kuang, PLoS Comput. Biol. **5**, e1000362 (2009).
[20] D. Ruiter *et al.*, Lancet Oncol., **3**, 35 (2002).
[21] H. M. Byrne and L. Preziosi, Math. Med. Biol. **20**, 341 (2003).
[22] V. Cristini *et al.*, J. Math. Biol. **58**, 723 (2008).
[23] E. de Angelis and L. Preziosi, Math. Models Methods Appl. Sci **10**, 379 (2000).
[24] C. Chatelain, P. Ciarletta and M. Ben Amar (to be published).
[25] L. D. Landau and L. M. Lifshitz, *Quantum Mechanics Non-Relativistic Theory, Third Edition* (Elsevier Science, Amsterdam, 1997).
[26] N. J. Poplawski *et al.*, Bull. Math. Biol., **71**, 1189 (2009).